International Journal of Engineering Trends and Technology
ISSN: 2231 – 5381 /doi:10.14445/22315381/IJETT-V69I12P210
Volume 69 Issue 12, 74-91, December, 2021

Underwater Sediment Layers analysis using Convnet with Adam Optimiser and mapping its reflection coefficient parameter with the Particle Size

Radhika Surampudi[1], Kumudham.R[2], Ebenezer Abishek.B[3], Rajendran.V[4]

[1,2,3,4]*Department of ECE,* [1,2,3,4]*School of Engineering,*
[1,2,3,4]*Vels Institute of Science, Technology and Advanced Studies, Pallavaram, Chennai, India*

[2]kumudham.rajamohan@gmail.com, [1]radhika.surampudi@gmail.com, [3]ebenezerabishek@gmail.com

Abstract *— Underwater sediment analysis is vital for cable and offshore installation, jet trenching, etc. Multiple pieces of research are performed for classifying the sea bed surface. Only fewer people focused on the classification of the sea bed sediment layers. Sub Bottom Profiler (SBP) equipment is utilized for imaging the seabed. SBP pings signal of low frequency and the signal is reflected back by the surface, while a portion of the signal penetrates through the surface and is reflected by the various layers of the sea bed. The sediment layers are classified using Convent with Adam Optimiser. The reflected signal contains information about the reflected object. The reflected coefficient is computed from classified sediment layers and is mapped to the density and particle size.*

Keywords *— Adam Optimiser, Classification, CNN, Convnet, Reflection, Sediment layer, Sub-bottom profiler.*

I. INTRODUCTION

Underwater imaging finds its applications in Cable and Pipeline Survey, Search and recovery, Land Mines detection, sub-bottom oil and gas surveys, Target verification and location, Archaeological Surveys, Geological/Geophysical Surveys, Marine Construction Surveys, Scour/Erosions Surveys for Rivers and Streams, Sediment Classification, etc. Pipelines underwater have been laid by Oil and Natural Gas industry. The surveillance and inspection of the pipelines for gas leakage or potable water leakage are achieved by underwater image processing. As well as the route for laying pipeline demands the need to know about the sediment types such as rock, clay, sand, etc. If there is any rock present, then the route should be diverted. The underwater image and seabed are captured by acoustic-based instruments carried by the remotely operated vehicle. Image processing underwater is achieved through Acoustic based instruments such as side-scan sonar equipment, with a frequency of 200 KHz. Side-scan sonar equipment captures images up to a depth of 75 m. Pipeline sometimes get buried underneath the sediments such as rock, sand, clay, etc., so subbottom profile equipment with frequency 10-12 KHz is used. Sub-bottom profiler capture image up to a depth of 20 m. In this work image captured by sub-bottom profile equipment is used.

Underwater image detection is an active area of research. But, the image detection is not clear. Sub Bottom Profiler (SBP) is a tool that is capable of identifying and classifying sediment layers of the seafloor. The SBP contains a transducer, which emits a low-frequency acoustic signal. The low-frequency acoustic signal is capable of penetrating through the surface of the seabed without much loss of the signal. Various portions of the acoustic signal are reflected by various sediment layers present underneath the seafloor, depending on the density of the material. The reflected signal contains information about the nature, such as density, of the reflected object. Therefore, by computing the reflection coefficient of the reflected signal, the reflected object can be identified and classified based on the data obtained.

II. LITERATURE SURVEY

Caulfield and Yim, 1983 [1] introduced new techniques for calculating the acoustic absorption coefficient in Ocean sediments. The model is similar to Hamilton's (1972) [2] research on seabed sediments. It is utilized for correcting losses in the bottom of the seabed so that the acoustic impedance and reflection coefficient from the sediment layers are computed. Outputs are obtained to show agreement with actual core data. Chivers et al., 1990 [3] developed an innovative method for echo-sounding signals processing. The fundamental concept, working, and pragmatic performance of the echo-sound signal instrument are effectively described. Utilizing data from the reflected sound waves, viewed through a receiver connected via the transducer terminal, earth differentiation is done with great success. The researchers installed the navigation system in a digital platform, and carried out a complete analysis, and showed the results on the chart.

Eleftherakis et al., 2012 [4] implemented methods using backscatter and depth residual features for improving riverbed sediment classification. Eleftherakis et al. (2012) [4] classified seabed and riverbed Sediment layers were utilizing multibeam echosounder data. The researchers made an analysis of the sediment classification output and acquired statistics using a multibeam echosounder on an experimental basis. The data is acquired from Sint Andries and Nijmegen at the Waal River. This is a follow-up to research work experimented with by Amiri-Simkooei et al. (2009) [5]. The attributes such as depth residuals and backscatter strength are selected utilizing principal component analysis. Principal components attribute is derived, and sediment is classified by clustering approach. The backscatter strength attributes differentiate between classes depending on the characteristics of sediment, and residual depth attributes differentiate classes depending on ripples from the river bed.

Guillon et al. (2001) [6] used the backscattering concept for buried sediment layer analysis. The authors experimented on (MBES) multi-beam echo-sounders signal of low-frequency. The signals from buried layers (up to the depth of a few meters) are affected by backscattering as well as by the penetration of sound into the sediment layers. This causes misinterpretation of the research information. The (EIBS) Equivalent Input Back Scattering Strength concept is applied, which deals with propagation inside fluid layer and local backscattering strength. At the upper interface, several results are summed to provide the backscattering strength. This featured various effects of attenuation and propagation in the sediment layer.

Hughes Clarke et al. (1997) [7] presented a method based on the grazing angle of the backscattered energies from the seabed. The angle response (AR) is characterized depending on slope vs. mean level and pre definite angle sector, and the absence or presence of rough variation in slope. The experiment is implemented to identify the existence of sediment frontier utilizing Angular Response extracted. The AR curves distinguishing frontier layers of sediments on Stellwagen Bank and Basin, Cape Race channel is attained. Orłowski, (1984) [8] presented a hydro-acoustic model for analysis of physical attributes of the seafloor. Multiple echoes interpreting the seafloor are analyzed and mapped to geological categories of the seafloor. A correlation was estimated between the multiple echoes from sea-bottom and morphological attributes of the seafloor. This model has been used for cartographic applications. Preston et al. (2004) [9] segmented the province of a survey are based on acoustic attributes. Geotechnical classification requires further non-acoustic information, in general. The authors applied Unsupervised clustering techniques to group into different classes. Bayesian clustering technique based on maximum-likelihood assignment is applied.

Sternlicht Daniel et al. (2003) [10] developed a model which is time-dependent for the acoustic backscattered energy from the seafloor. The data is collected from echo-sounder operating at 33 and 93 kHz. Energy scattered from the sediment layer is analyzed using Helmholtz-Kirchhoff theory which reflects the average grain size, reflection coefficient, and the roughness power spectrum. The authors applied Jackson et al. [J. Acoust. Soc. Am. 79, 1410-1422 (1986)] [11], roughness approach for predicting backscattering from the bottom of the seafloor. It includes the sediment's attenuation coefficients, volume scattering, the interface between sound and the sediment. The estimated parameters characterize ambiguous ranges of two spectral components. The output analysis yielded better results for sediment classification based on roughness spectrum parameters.

Theuillon et al., 2008[12] characterized the seabed using acoustic attributes. Sub-bottom profilers are utilized to analyze the topmost sediment layers beneath the ocean bed. The author's estimated geo-acoustic parameters such as reflectivity, absorption, and impedance, contrast. The proposed Calibration Methodology is tested against real data collection during the (CALIMERO) experiment for analysis of the sea bed. It is shown that the estimated parameters are consistent with real-time attributes of sediment layers. Berthold et al. (2017) [17] applied the CNN model on sonar images for performing sediment classification as four types like coarse, sand, fine, and mixed sediment automatically. During sand prediction, accuracy measures as 83%, mixed sediment as 11%, which reaches bad accuracy in sediment classification. Xiangjin Ran et al. (2019)[18] introduced an image analysis-based deep CNN approach for finding the kind of rock and performed classification, which attains an accuracy of 98%. Pierre Guy Atangana Njock et al. (2020)[19], in their review, emphasized the need for sediment classification for jet trenching.

Berthold et al. [21] applied the CNN model on sonar images for performing sediment classification as four types like coarse, sand, fine, and mixed sediment automatically. During sand prediction, accuracy measures as 83%, mixed sediment as 11%, which reaches bad accuracy in sediment classification. Chen et al. [22]Initially applied the denoising technique to remove the unwanted noises from sonar images so as to extract the statistical, texture, and also gray feature along with segment reliability. Subsequently, the author presented an algorithm, namely a multi-class Support Vector Machine, for fragmenting the sub-aquatic dregs (sediment) sonar image. This algorithm attains better outcomes with a superior detection rate. Dell'Aversana et al. [23] found that categorization of rock is reliable by constructing a machine learning structure along with its workflow based on a mineralogical and compound constitution. The structure made by the machine learning technique is helpful to lithologists as well as geological operations. Baraboshkin et al. [24] introduced an approach, namely CNN-based algorithms such as ResNet, VGG, GoogleNet, and AlexNet, in which finding rocks from sediment needed a lesser amount of time to facilitate the geologist to work very effectively and efficiently. Moreover, they explained some approaches based on analysis of color distribution as well as extraction

of relevant attributes. Frederick et al. [25] used machine learning algorithms attached with model-based Approaches for categorizing dregs in acoustics surroundings based on properties of sub-aquatic. Here, they applied with low-frequency model and high-frequency model for finding the spreading of sediments by layers.

III. EXISTING METHOD

A time-domain energy prototype has been developed to classify the sediment layers. The received energy signal is calculated in sequence by computing the acoustical criterion of the sediment layers. The received energy signal constitutes the backscattering and reflection, which represents only impedance contrast and not the roughness of the material.

The existing model focus on the backscattered intensities and single reflection from the sediment layers [20]. It did not consider multiple reflections from different sediment layers. Previous methods also focused on absorption coefficient parameters.

IV. METHODOLOGY

The purpose of this work is to classify the sediment layers and analyze them based on the reflection coefficient computed from the image captured by the Sub Bottom Profiler[15]. Classification is done using Convnet with adam optimization algorithm. The reflection coefficient is computed from the classified sediment layers for analysis. The obtained reflection coefficient of the image is then mapped to their corresponding density values and particle size.

The image captured by the SBP is the energy distribution of the reflected signal. Hence, the image is converted into numerical data for processing the data. The input image is partitioned into smaller bins for ease of processing the data. The size of the bin can be chosen according to the need of the user. To avoid intermediate values present in the data, the obtained data is quantized, which eases the processing of the data, and then it is classified using Convnet with Adam optimization algorithm. The reflection coefficient of the obtained image is computed for extracting the information regarding the density of the sediment materials. The calculated reflection coefficient is mapped to the density of the corresponding material. The particle size is directly proportional to the density of the object.

A. Indian Standard Particle Size Classification:

The particle or grain size classification approved by the Bureau of Indian Standards (BIS; earlier called the Indian Standard Institution, ISI) is illustrated in Fig 1. In this system, soil particles are classified into gravel, sand, silt, and clay.

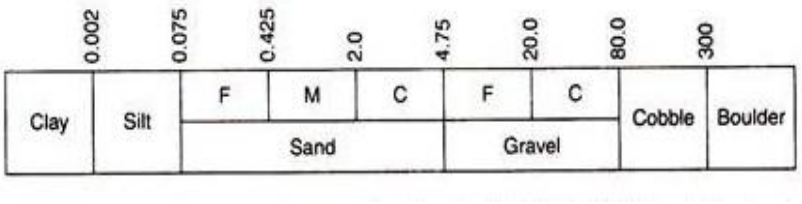

Fig 1. Indian Standard Particle Size Classification(IS:1498-1970)(Particle size in mm)

Legend:F = Fine, C = Coarse, M = Medium, VC = Very Coarse

As per the Indian standard particle size classification, clay has a grain size < 0.002 mm. Silt is coarser than clay, with a grain size of 0.002-0.075 mm. Sand, with a grain size of 0.075-4.75 mm, is subdivided into fine, medium, and coarse, as shown in Fig. 1. Gravel is coarser than sand and has a particle size of 4.75-80 mm. Particles coarser than gravel are called cobble, with a particle size of 80-300 mm, and boulder, which is coarser than cobble and has a particle size > 300 mm.

(Ref:http://www.soilmanagementindia.com/soil/soil-classification/basis-of-soil-classification/13460)[13]

Based on the particle size of the data computed, various colors are assigned. These colors are then mapped into an image.

The size of the particle is directly proportional to the reflection coefficient. Since the reflection coefficient varies between 0 and 1. The interval 0 to 1 is divided into sub-intervals, and the image is mapped according to the interval to which the value of the reflection belongs.

B. DATASET

The raw sonar data is collected from Indomer Coastal Hydraulics Pvt Ltd. The study area investigated is Perur, Chennai, Tamil Nadu. The data was recorded using BENTHOS SIS-1600 side scan sonar with a frequency of 10 KHz.

C. Sub Bottom Profile Equipment

Sub Bottom Profiler (SBP) is a tool that is capable of identifying and classifying sediment layers of the seafloor. The SBP contains a transducer, which emits a low-frequency acoustic signal. The low-frequency acoustic signal is capable of penetrating through the surface of the seabed without much loss of the signal. Various portions of the acoustic signal are reflected by various sediment layers

present underneath the seafloor, depending on the density of the material. The reflected signal contains information about the nature, such as density, of the reflected object. Therefore, by computing the reflection coefficient of the reflected signal, the reflected object can be identified and classified based on the data obtained. Computing the reflection coefficient of the reflected signal, the reflected object can be identified and classified based on the data obtained.

Fig 2. CAP 6600 CHIRP II Acoustic Sub-Bottom Profiler

Fig 3. Location of the Investigation area in the Bay of Bengal Sea

The Sub-bottom profiling system CAP 6600 Chirp III Acoustic Sub-Bottom Profiler shown in Fig 2 is ideal for identifying and characterizing layers of sediment or rock under the seafloor. This instrument will satisfy the industry's requirement of a long-range Chirp sub-bottom profiler. Compressed High-Intensity Radiated Pulse technology helps to produce sub-bottom layer images with high resolution. Although traditional systems have provided acceptable penetration and resolution, the capability to provide required levels of improved resolution and range are the constraints still faced by the researchers.

The location of the investigation area Perur is shown in Fig 3 and is sited at the Bay of Bengal. The area covered is (3 x 2.5) Km^2. The image is taken at a distance of 440 m from the land area calculated using Haversine Formula kumudham et al. (2018)[14]. A portion of the subbottom image is shown in Fig 4, where sediment analysis is done.

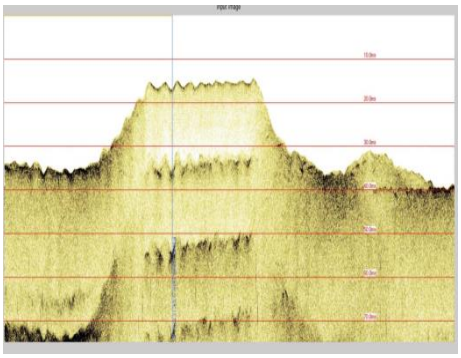

Fig 4. Sub Bottom Profiler Image

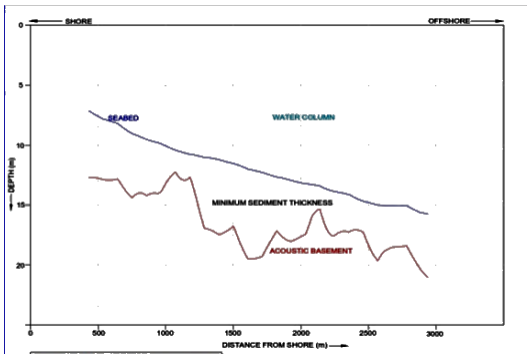

Fig 5. Sediment Thickness

The sediment thickness layer between 2m and 4 m below the seabed is taken for analysis Fig 5. The spike on the acoustic basement indicates the presence of hard strata.

V. METHODOLOGY FLOW

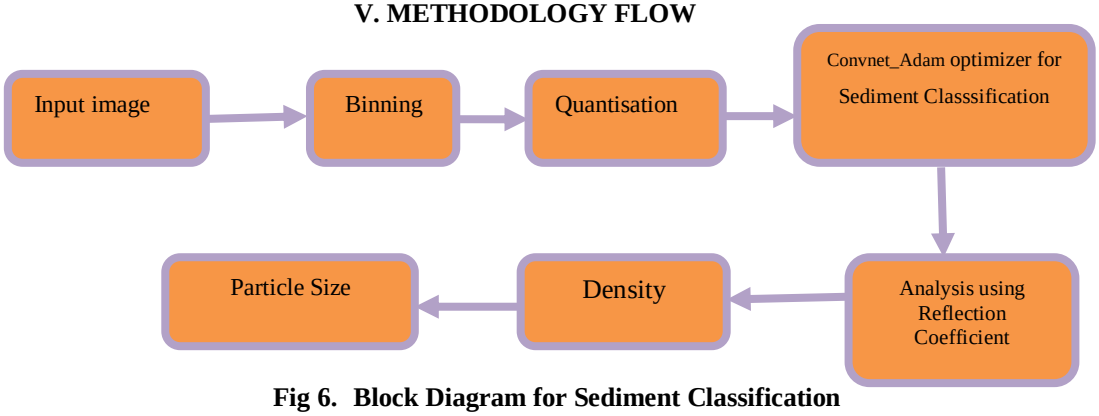

Fig 6. Block Diagram for Sediment Classification

The purpose of this work is to classify sediment layers using Deep learning Convnet with adam optimizer and analyze based on the reflection coefficient computed from the sediment image captured by the SubBottom Profiler. The classified layers are mapped to their corresponding density values and to the particle size (Fig 6).

A. Input Image

The input image (Fig 7) is obtained from sub-bottom profiling Equipment. The image captured by the SBP is the energy distribution of the reflected signal. Hence, the image is converted into numerical data for processing the data.

B. Binning

The input image is segmented into smaller segments for ease in processing the data. The size of the bin can be chosen according to the need of the user.

C. Quantization

To avoid intermediate values present in the data, the obtained data is quantized, which eases the processing of the data.

D. Classification

The segmented layers are classified using Convnet with Adam Optimiser.

E. Reflection Coefficient

The reflection coefficient of the obtained image is computed [15] for extracting the information regarding the density of the sediment materials.

F. Density

The calculated reflection coefficient is related to the density of the corresponding material using the relation,

a) Density ∝ reflection coefficient.

1) Particle Size

The particle size is directly proportional to the density of the object. This clearly states that if the density of the material is more, the particle size is large. Based on the particle size of the data computed, various colors are assigned. These colors are then mapped into an image.

2) Image Binning

The size of the image captured by the SBP is very large. It is very difficult to process such huge data. Hence, the input image is partitioned into smaller segments. The size of the segmentation of the input image is fixed, but it can be varied depending on the application. The input image is with the dimension 1270 x 577. A portion of the image shown in Fig 7 for analysis is taken.

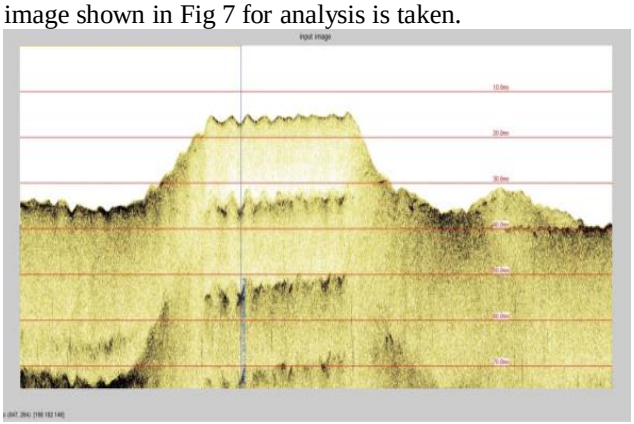

Fig 7. Input image from Sub Bottom Profiler

3) Quantization

The whole image is subdivided. Each binned image shown in Fig 8 is quantized separately so that there isn't any intermediate value present in the data. The quantized data is represented in numerical values. The binned Block 8 is taken for analysis.

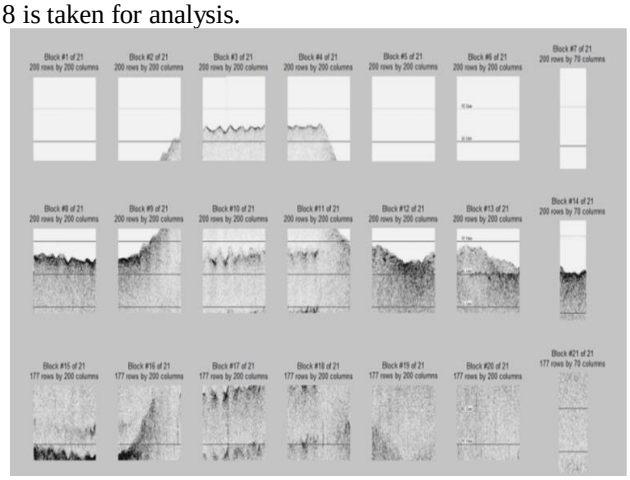

Fig 8. Binned Image

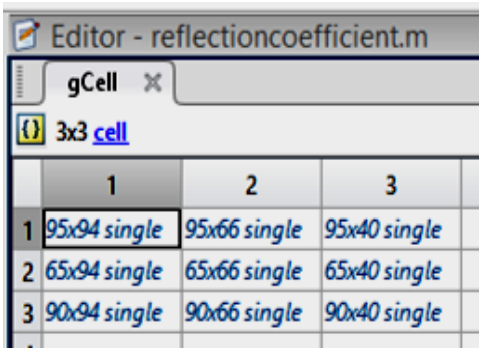

Fig 9. Quantized Bins

Fig 9 shows the bins which have quantized values.

gCell =

[95x94 single]	**[95x66 single]**	**[95x40 single]**
[65x94 single]	**[65x66 single]**	**[65x40 single]**
[90x94 single]	**[90x66 single]**	**[90x40 single]**

For the bin value of size [95x94 single], the quantized values (250x200) are shown in Fig 10, which divides the image into different intensity levels.

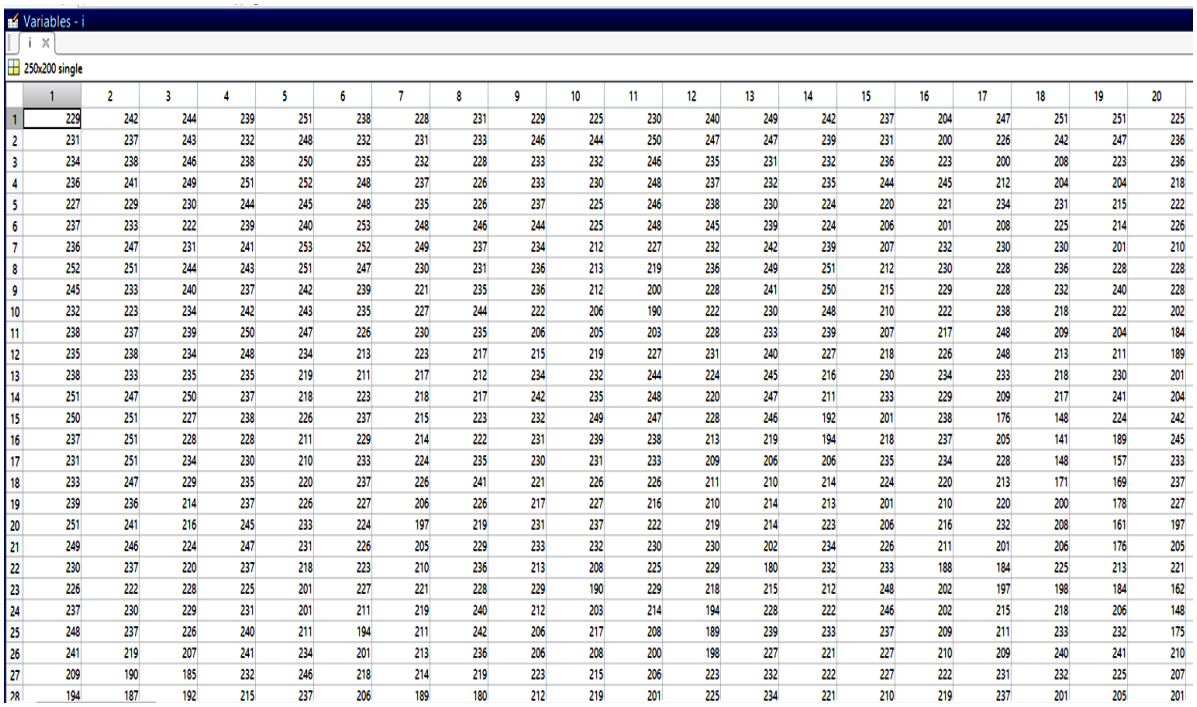

	1	2	3	4	5	6	7	8	9	10	11	12	13	14	15	16	17	18	19	20
1	229	242	244	239	251	238	228	231	229	225	230	240	249	242	237	204	247	251	251	225
2	231	237	243	232	248	232	231	233	246	244	250	247	247	239	231	200	226	242	247	236
3	234	238	246	238	250	235	232	228	233	232	246	235	231	232	236	223	200	208	223	236
4	236	241	249	251	252	248	237	226	233	230	248	237	232	235	244	245	212	204	204	218
5	227	229	230	244	245	248	235	226	237	225	246	238	230	224	220	221	234	231	215	222
6	237	233	222	239	240	253	248	246	244	225	248	245	239	224	206	201	208	225	214	226
7	236	247	231	241	253	252	249	237	234	212	227	232	242	239	207	232	230	230	201	210
8	252	251	244	243	251	247	230	231	236	213	219	236	249	251	212	230	228	236	228	228
9	245	233	240	237	242	239	221	235	236	212	200	228	241	250	215	229	228	232	240	228
10	232	223	234	242	243	235	227	244	222	206	190	222	230	248	210	222	238	218	222	202
11	238	237	239	250	247	226	230	235	206	205	203	228	233	239	207	217	248	209	204	184
12	235	238	234	248	234	213	223	217	215	219	227	231	240	227	218	226	248	213	211	189
13	238	233	235	235	219	211	217	212	234	232	244	224	245	216	230	234	233	218	230	201
14	251	247	250	237	218	223	218	217	242	235	248	220	247	211	233	229	209	217	241	204
15	250	251	227	238	226	237	215	223	232	249	247	228	246	192	201	238	176	148	224	242
16	237	251	228	228	211	229	214	222	231	239	238	213	219	194	218	237	205	141	189	245
17	231	251	234	230	210	233	224	235	230	231	233	209	206	206	235	234	228	148	157	233
18	233	247	229	235	220	237	226	241	221	226	226	211	210	214	224	220	213	171	169	237
19	239	236	214	237	226	227	206	226	217	227	216	210	214	213	201	210	220	200	178	227
20	251	241	216	245	233	224	197	219	231	237	222	219	214	223	206	216	232	208	161	197
21	249	246	224	247	231	226	205	229	233	232	230	230	202	234	226	211	201	206	176	205
22	230	237	220	237	218	223	210	236	213	208	225	229	180	232	233	188	184	225	213	221
23	226	222	228	225	201	227	221	228	229	190	229	218	215	212	248	202	197	198	184	162
24	237	230	229	231	201	211	219	240	212	203	214	194	228	222	246	202	215	218	206	148
25	248	237	226	240	211	194	211	242	206	217	208	189	239	233	237	209	211	233	232	175
26	241	219	207	241	234	201	213	236	206	208	200	198	227	221	227	210	209	240	241	210
27	209	190	185	232	246	218	214	219	223	215	206	223	232	222	227	222	231	232	225	207
28	194	187	192	215	237	206	189	180	212	219	201	225	234	221	210	219	237	201	205	201

Fig. 10 Quantized Values

4) Classification Using Convnet with Adam optimizer

The model was evaluated on both training and testing phases using Convnet with Adam optimizer described in Table 1. To attain better performance based on accuracy measures, we are tuning the learning rate parameter up to 100 epochs for validating both losses as well as accuracy.

TABLE 1. Model evaluation with varied learning rate

Model	Learning Rate 0.01		Learning Rate(0.02)		Learning Rate(0.03)	
	Train	Test	Train	Test	Train	Test
CNN with Adam optimizer	94.02	88.13	92.89	90.12	94.80	90.27
CNN with Adam optimizer	81.16	79.90	80.89	84.17	83.13	83.12
CNN with Adam optimizer	87.38	87.62	93.59	89.72	93.65	90.16

By using sonar images, we are identifying the sediment particles and further undergo classification for isolating rocks from clay, mud, and every other sediment particle. The following Fig 11 illustrates that solid lines represent the division of sand from the rock using different CNN techniques along with varied learning rate/batch size.

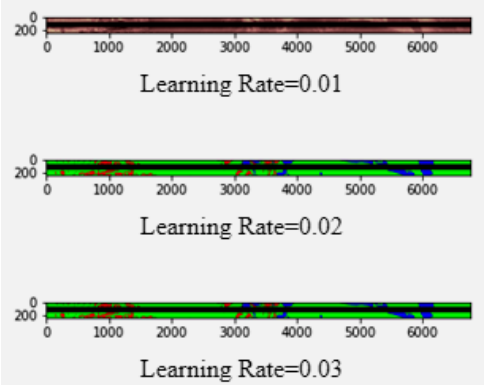

Fig. 11 Sediment classification by solid lines

Model Evaluation

SediDeep model is evaluated for classifying the sediments into rocks, sands, and others via estimating learning rates as 0.01, 0.02, and 0.03. The image specification of classified sediment images with varied learning rates is illustrated in Fig 12.

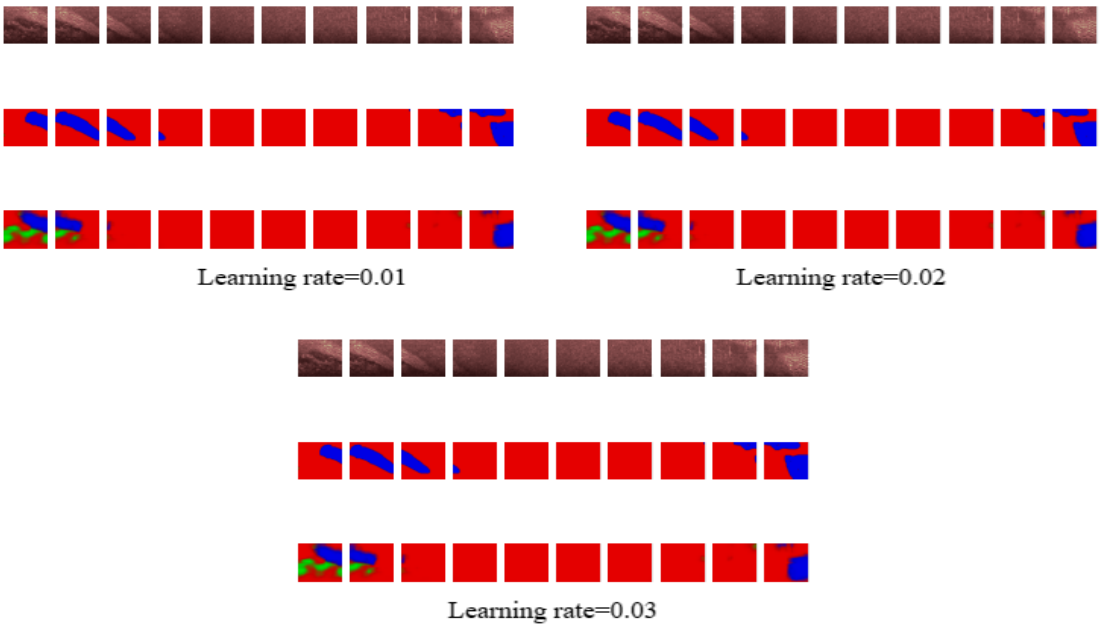

Fig. 12 Image specification in classifying sediments

Experimental Outcomes

The training phases occupy arbitrary preliminary weights. After the finishing of every batch size, the learning rate also varies; the weights are continuously in tuning to locate the finest (optimal) value that may decrease the training phase loss value. Subsequent to every epoch, the parameters which are trained should keep in one file that is utilized to estimate the validation dataset and attain detection accuracy. We analyzed the sub-aquatic sediments on sonar images with 100 epochs to estimate the validation dataset and achieve accuracy in the detection and classification of sediments as rocks, clays, mud, and others.

Adam optimizer with learning rate 0.01

The two metrics, namely loss and accuracy during the evaluation under training phase, using Adam optimizer with learning rate as 0.01. The graph representations for both metrics are shown in Fig 13 and 14.

Adam optimizer with learning rate 0.02

To evaluate the performance of identifying the sediments available on acoustic images and categorizing the sediment particles into sands, clay, mud, etc., and most effective metrics need to be estimated, namely accuracy measure. Thus we evaluate accuracy metrics for several epochs for training the images and finally validating the results. Here, we trained the images using the CNN-based Adam optimizer technique along with the learning rate 0.02 graph depicted in Fig 15 and 16. The x dimensions represent the number of epochs, whereas the y dimensions represent accuracy/loss.

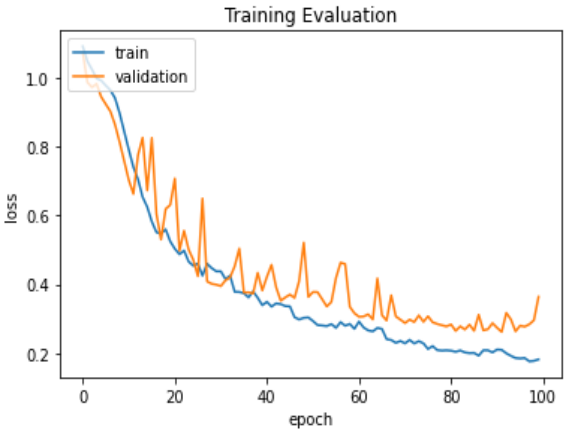

Fig. 13 Evaluate Loss during training and validation

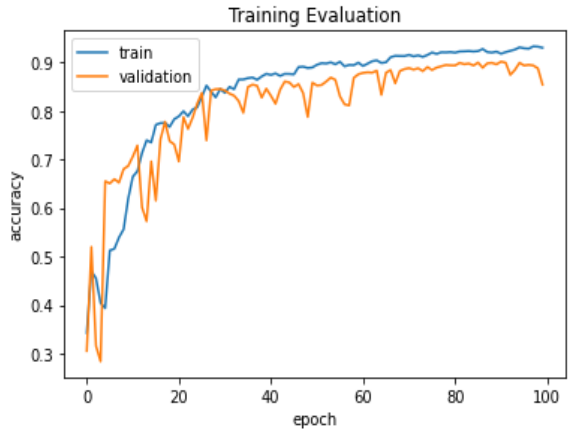

Fig. 14 Accuracy graph for training and validation phase

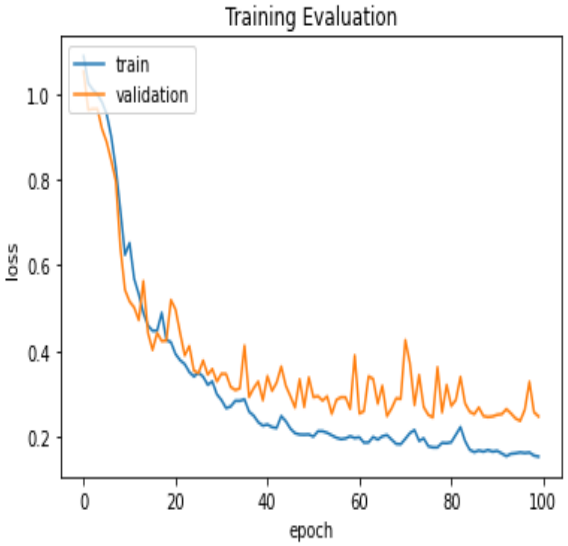

Fig 15. Loss metric with Lr=0.02

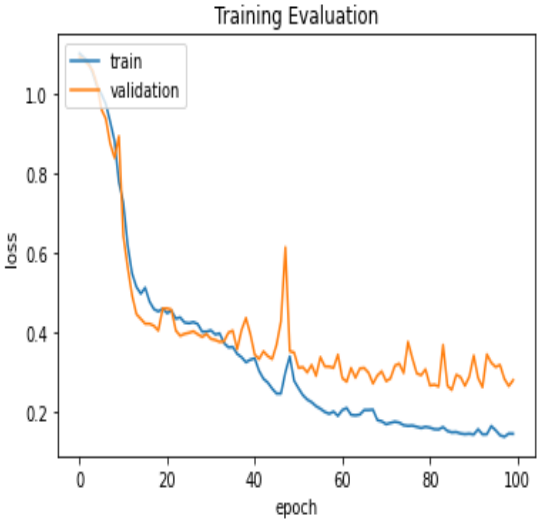

Fig 17. Training and validation graph for loss metric

Fig 16. Accuracy estimation graph for training and validation with Lr=0.02

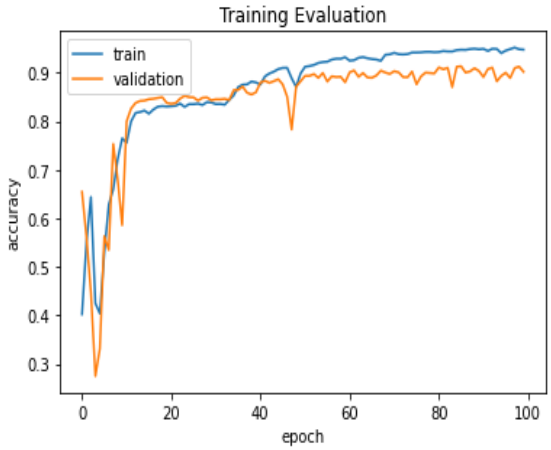

Fig 18. Training and validation graph for accuracy metric

Adam optimizer with learning rate 0.03

The graph represents the plotting of the number of epochs versus accuracy/loss under training and also validation depicted in Fig 17 and 18 using Adam optimizer with learning rate 0.03 to obtain the optimal values for predicting the model performance.

Analysis of Pixels using Reflection Coefficient parameter in the classified Sediment Layers

The reflection coefficient is defined as the ratio of actual intensities to maximum intensities, and it is denoted as 'R'.

Reflection coefficient (R) ∝ Density

Each pixel in the input image is divided by the maximum intensity value, i.e., 255, which gives the reflection coefficient. Generally, the calculated reflection coefficient varies between 0 and 1 shown in Fig 19, 20. The reflection coefficient of a particular range that distinguishes the sediment layers is shown below. This depends on the nature of the material, either rough or smooth, based on reflectivity.

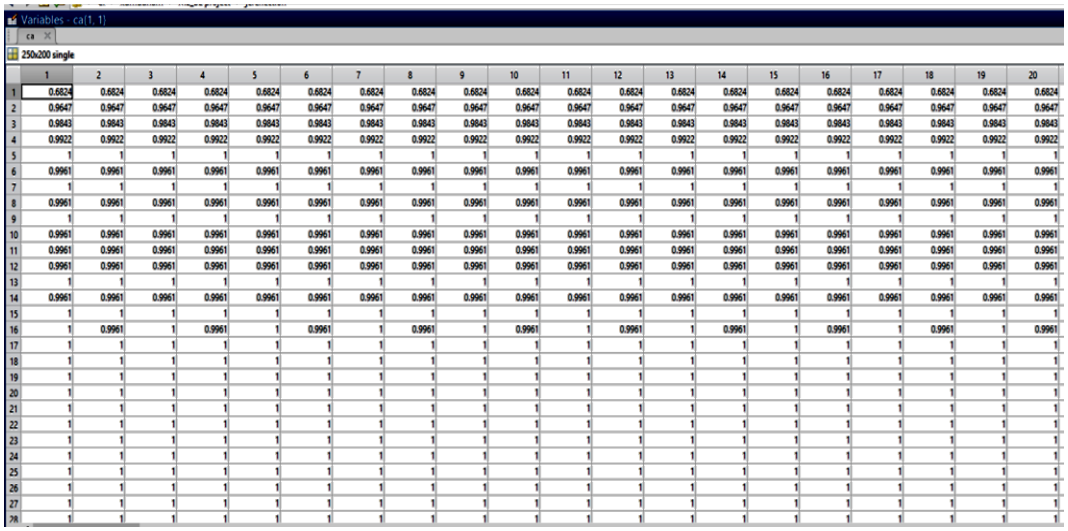

Fig 19. Calculated Reflection Coefficient[15]

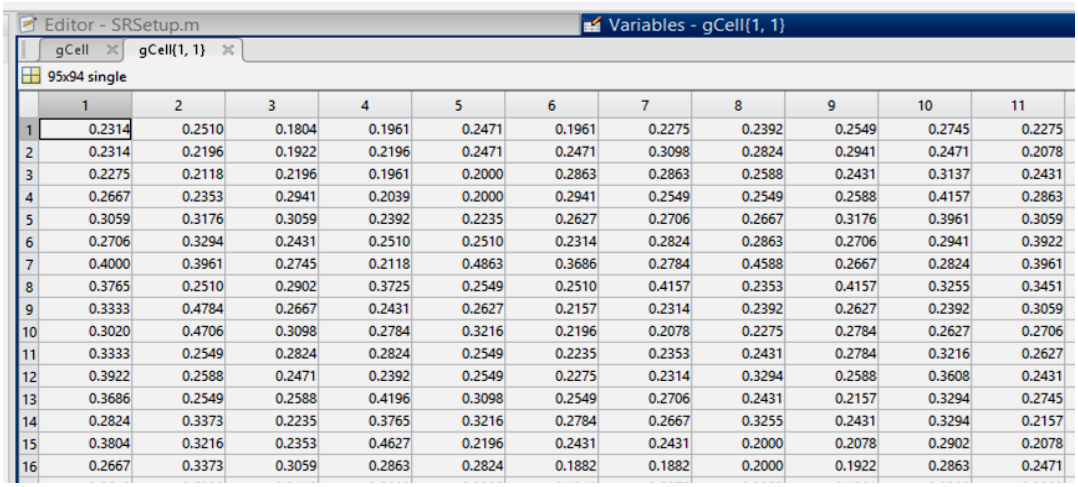

	1	2	3	4	5	6	7	8	9	10	11
1	0.2314	0.2510	0.1804	0.1961	0.2471	0.1961	0.2275	0.2392	0.2549	0.2745	0.2275
2	0.2314	0.2196	0.1922	0.2196	0.2471	0.2471	0.3098	0.2824	0.2941	0.2471	0.2078
3	0.2275	0.2118	0.2196	0.1961	0.2000	0.2863	0.2863	0.2588	0.2431	0.3137	0.2431
4	0.2667	0.2353	0.2941	0.2039	0.2000	0.2941	0.2549	0.2549	0.2588	0.4157	0.2863
5	0.3059	0.3176	0.3059	0.2392	0.2235	0.2627	0.2706	0.2667	0.3176	0.3961	0.3059
6	0.2706	0.3294	0.2431	0.2510	0.2510	0.2314	0.2824	0.2863	0.2706	0.2941	0.3922
7	0.4000	0.3961	0.2745	0.2118	0.4863	0.3686	0.2784	0.4588	0.2667	0.2824	0.3961
8	0.3765	0.2510	0.2902	0.3725	0.2549	0.2510	0.4157	0.2353	0.4157	0.3255	0.3451
9	0.3333	0.4784	0.2667	0.2431	0.2627	0.2157	0.2314	0.2392	0.2627	0.2392	0.3059
10	0.3020	0.4706	0.3098	0.2784	0.3216	0.2196	0.2078	0.2275	0.2784	0.2627	0.2706
11	0.3333	0.2549	0.2824	0.2824	0.2549	0.2235	0.2353	0.2431	0.2784	0.3216	0.2627
12	0.3922	0.2588	0.2471	0.2392	0.2549	0.2275	0.2314	0.3294	0.2588	0.3608	0.2431
13	0.3686	0.2549	0.2588	0.4196	0.3098	0.2549	0.2706	0.2431	0.2157	0.3294	0.2745
14	0.2824	0.3373	0.2235	0.3765	0.3216	0.2784	0.2667	0.3255	0.2431	0.3294	0.2157
15	0.3804	0.3216	0.2353	0.4627	0.2196	0.2431	0.2431	0.2000	0.2078	0.2902	0.2078
16	0.2667	0.3373	0.3059	0.2863	0.2824	0.1882	0.1882	0.2000	0.1922	0.2863	0.2471

Fig 20. Calculated Reflection Coefficient[15]

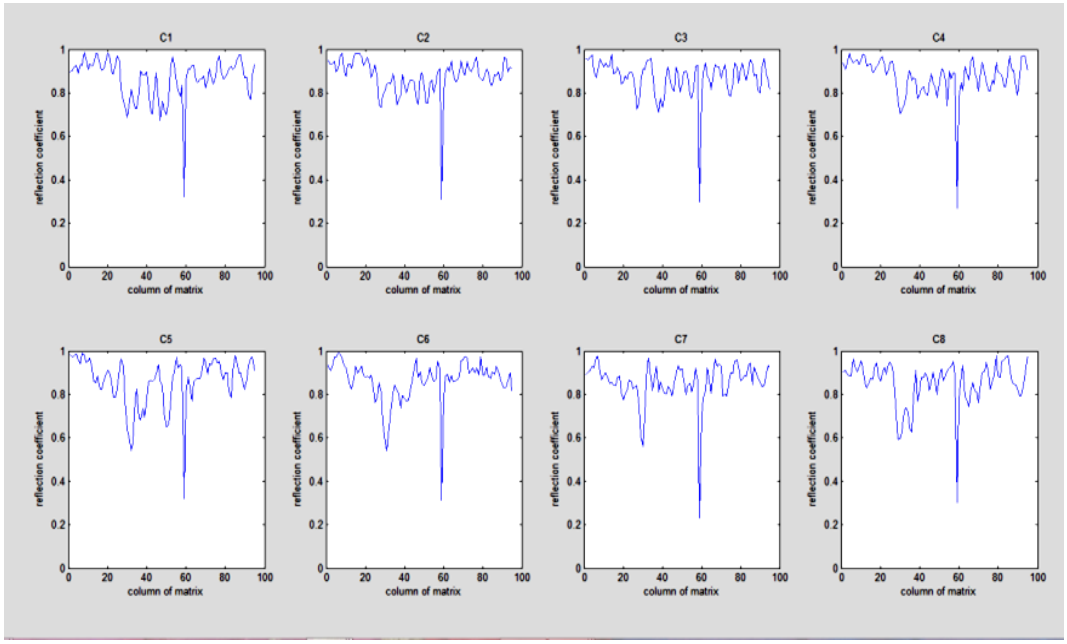

Fig 21. Reflection coefficient Graph (Range 0.9-1)

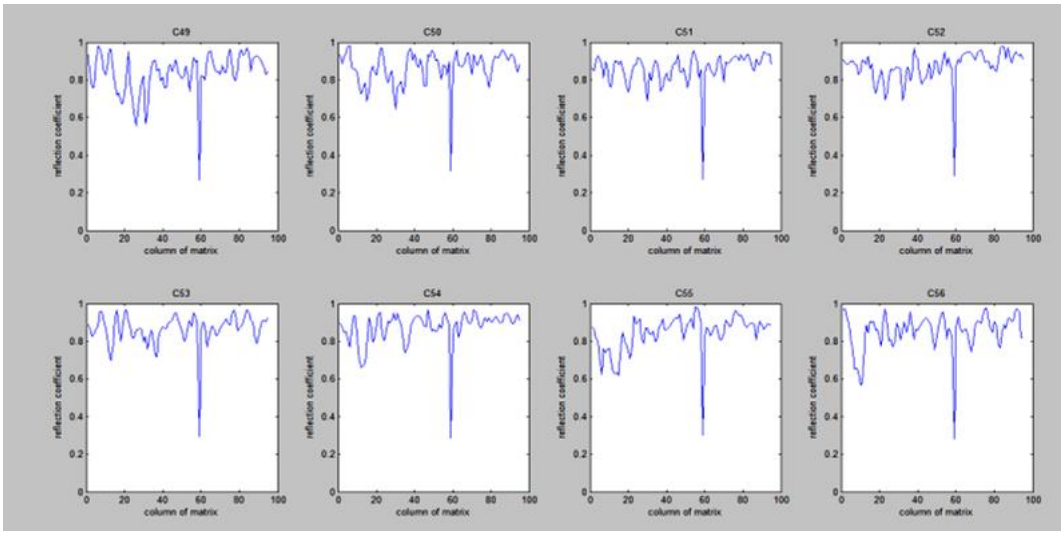

Fig 22. Reflection coefficient Graph (Range 0.9-1)

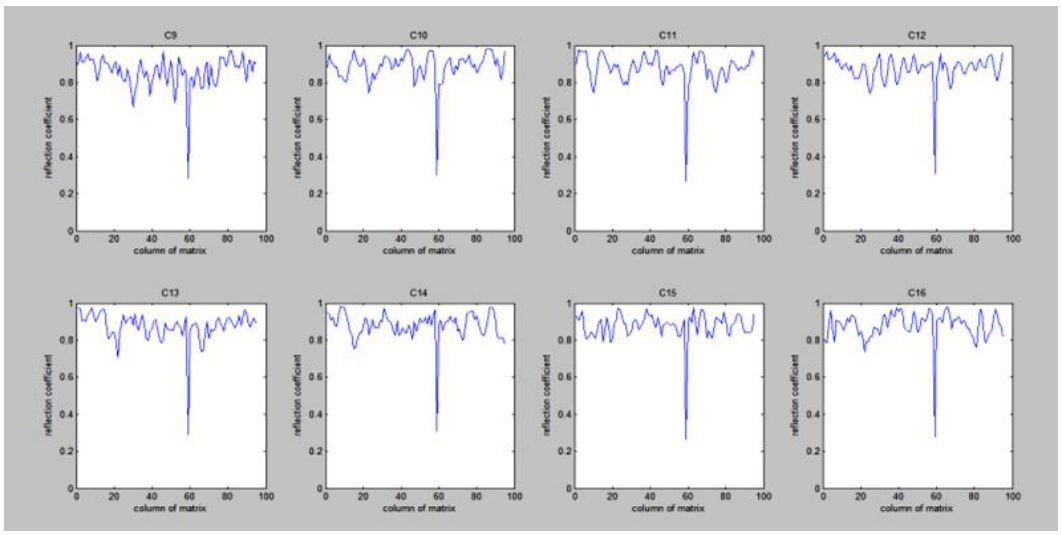

Fig 23. Reflection coefficient Graph (Range 0.8-0.9)

Reflection coefficient Graph is plotted for each column shown in Fig 21, 22, 23 Range 0.8 to 1. The high Reflection coefficient approximately is mapped with Rock of large particle size showing roughness characteristics.

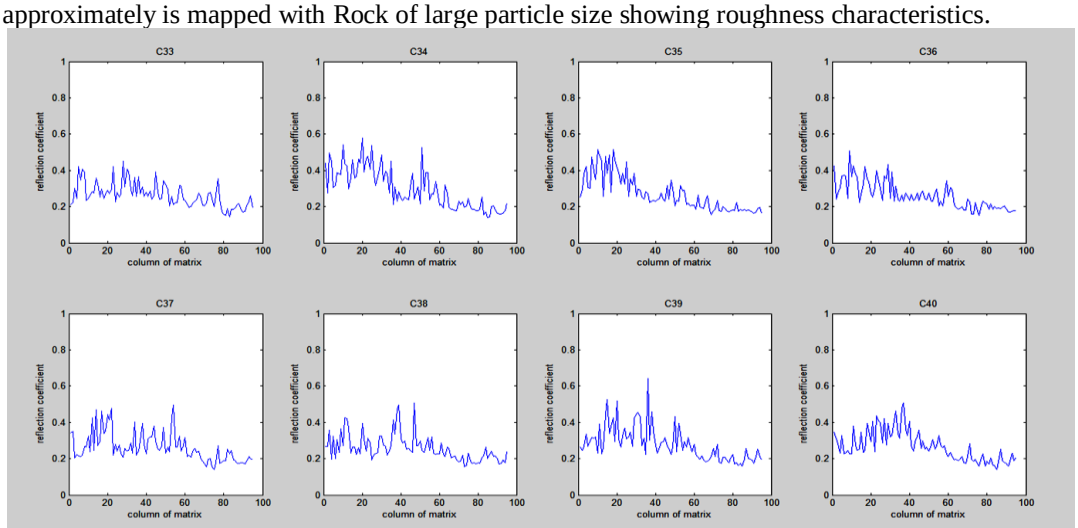

Fig 24. Reflection coefficient Graph (Range 0.3 - 0.4 Sandy Clay)

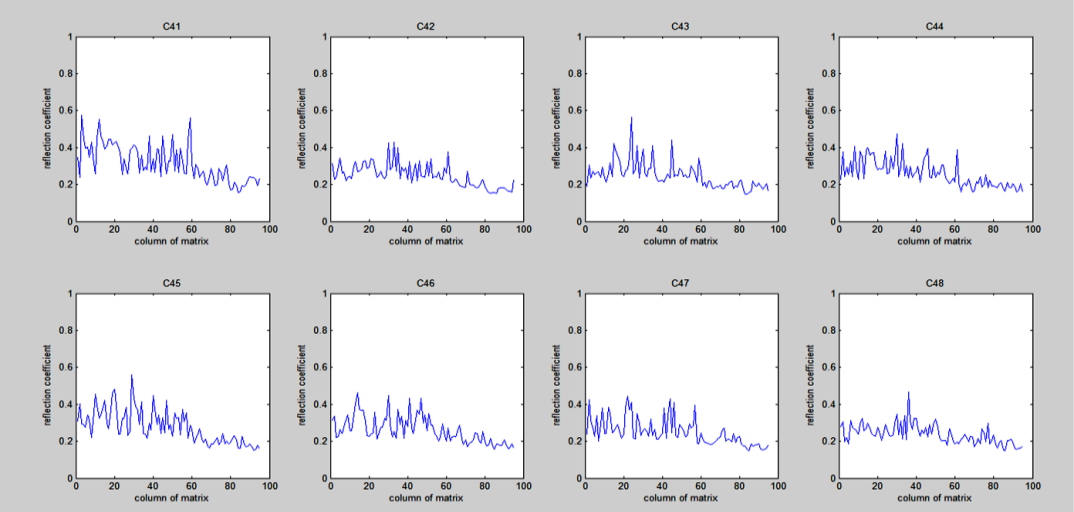

Fig 25. Reflection coefficient Graph (Range 0.3-0.4)

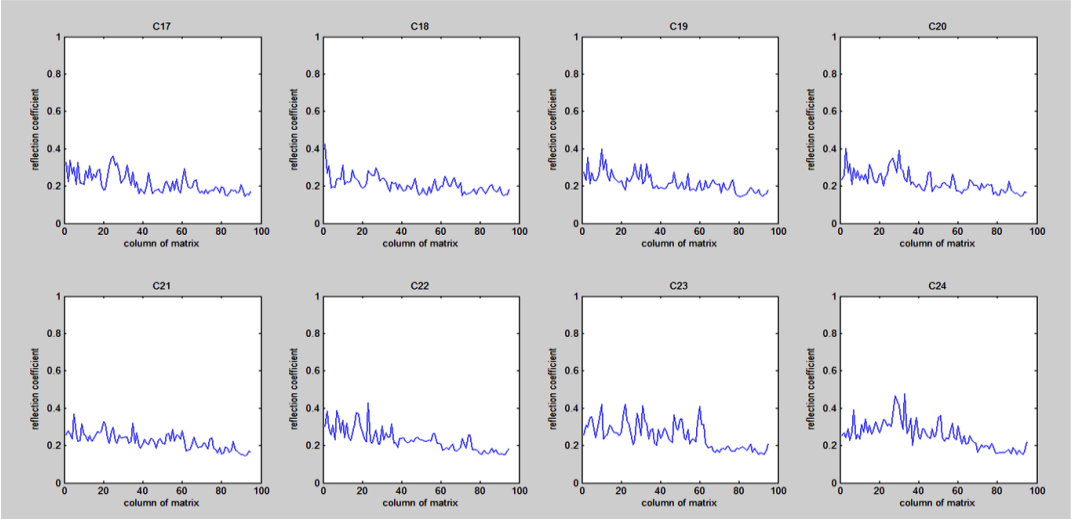

Fig 26. Reflection coefficient Graph (Range 0.3-0.4)

Reflection coefficient Graph is plotted for each column illustrated in Fig 24, 25, 26 shows the Range 0.3 to 0.4. This Reflection coefficient is approximately mapped with Sandy Clay characterizing smoothness.

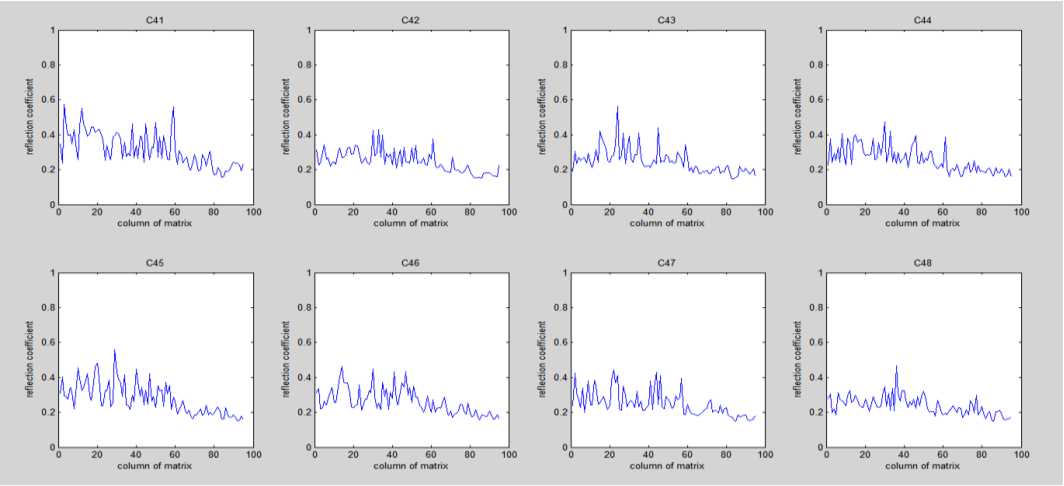

Fig 27. Reflection coefficient Graph (Range 0.2 -0.3 clayey sand)

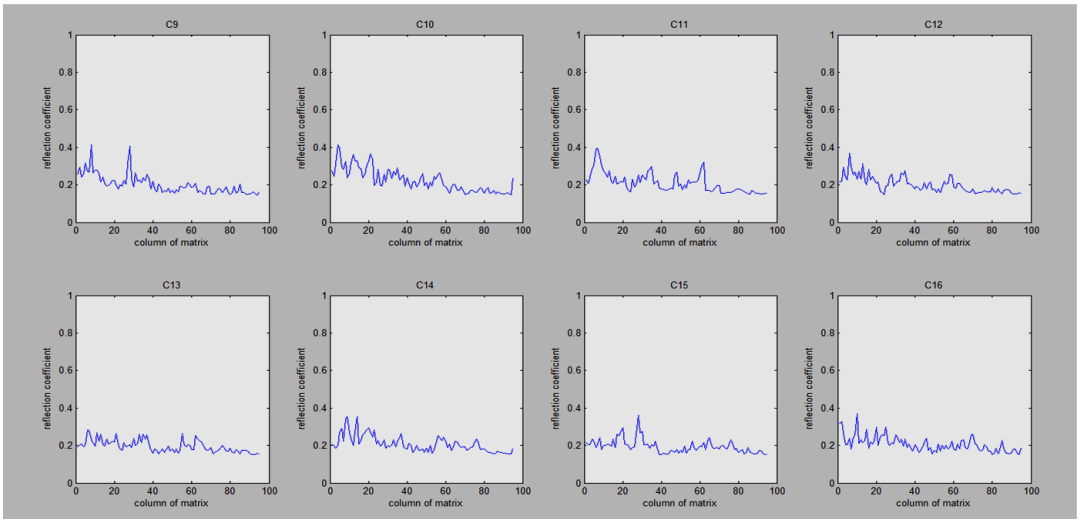

Fig 28. Reflection coefficient Graph (Range 0.2 -0.3 clayey sand)

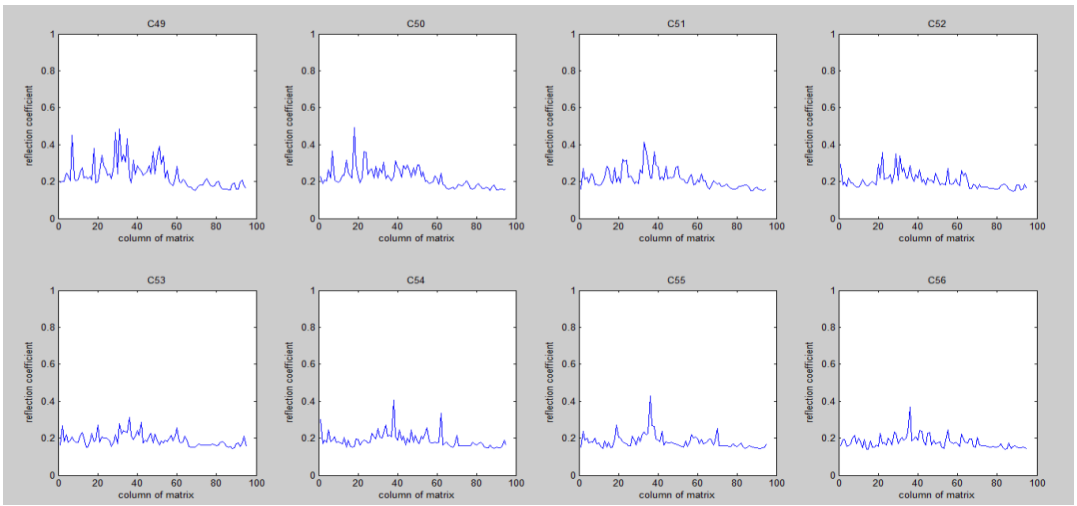

Fig 29. Reflection coefficient Graph (Range 0.2 -0.3 clayey sand)

Reflection coefficient Graph is plotted for each column illustrated in Fig 27, 28, 29 shows the Range 0.2 to 0.3. This Reflection coefficient is approximately mapped with Clayey Sand.

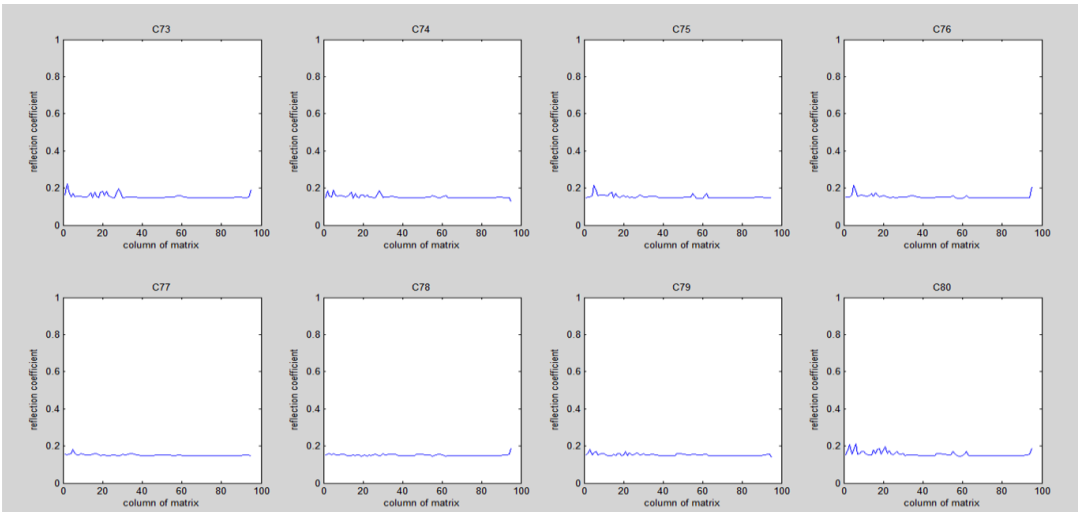

Fig 30. Reflection Coefficient Graph (Range 0.19-0.2)

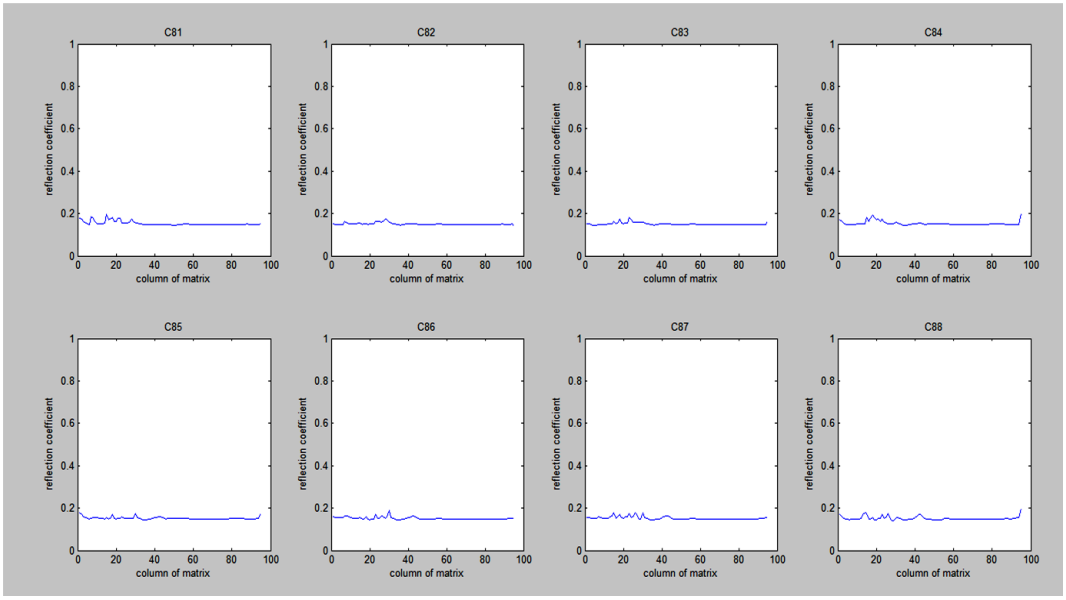

Fig 31. Reflection Coefficient Graph (Range 0.19-0.2)

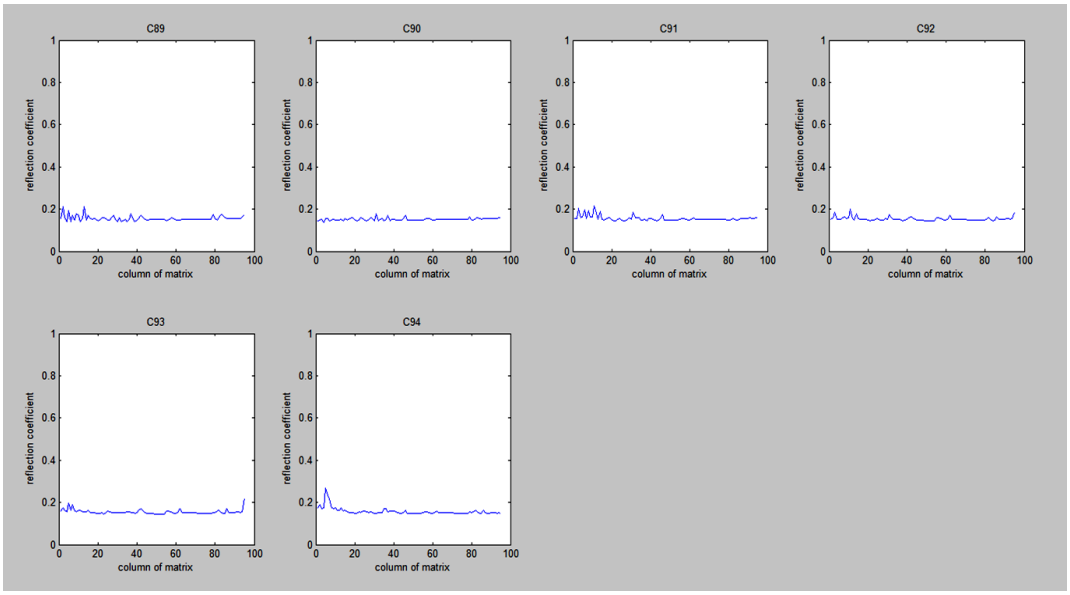

Fig 32. Reflection Coefficient Graph (Range 0.19-0.2)

Reflection coefficient Graph is plotted for each column illustrated in Fig 30, 31, 32 shows the Range 0.19 to 0.2. This Reflection coefficient is approximately mapped with Clay. In some graphs, overlapping ranges, as well as high peaks, are viewed. This is a due mixture of soil such as sandy clay or clayey sand.

PARTITIONING OF SEDIMENT LAYERS

The reflection coefficient of the sediment layers is put into ranges varying from 0 to 1. The different layers of similar attributes but with different particle sizes are color mapped based on the reflection coefficient. The final classification of Sediment layers are obtained by mapping the ranges of particle size with the assigned color. Fig 33 shows the partitioning of the sediment layers based on reflection coefficient attributes so that they are well distinguished from one another. (kumudham et al. 2017)[15].

The Reflection Coefficient graph (Fig 19-32) infers the high reflection coefficient is from large particle size. The same is given in Table 2.

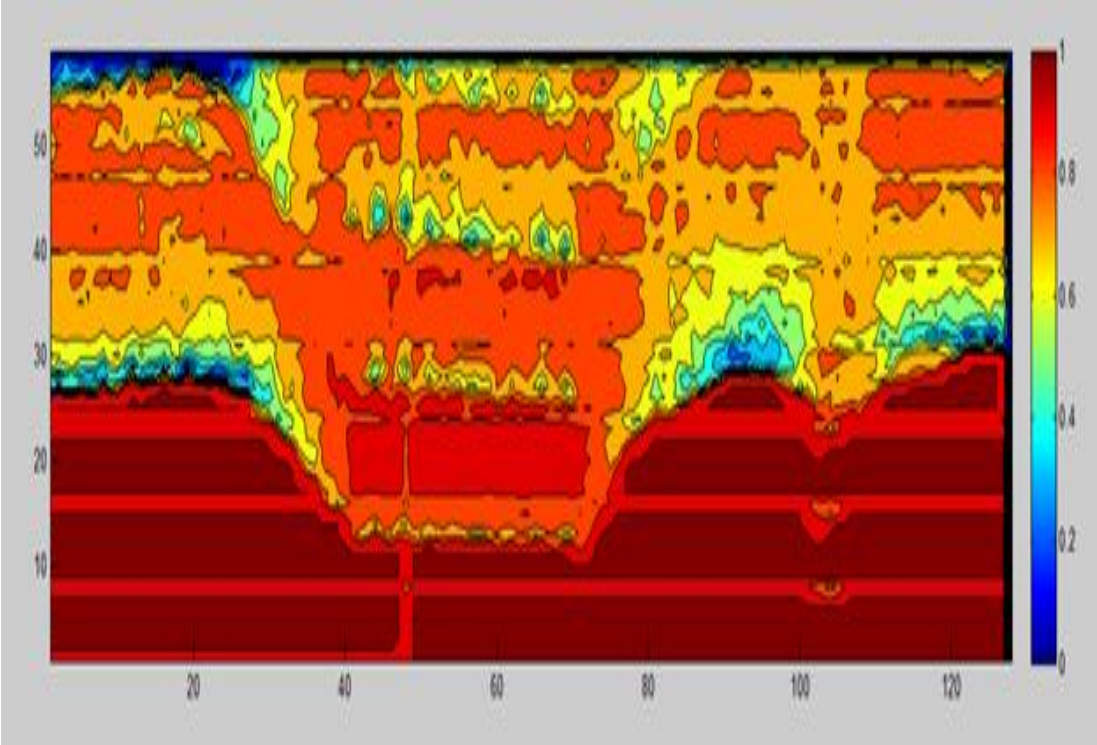

Fig 33. Colour Mapping of Sediment Layers[15]

Density

The density and reflection coefficient is directly proportional to each other. For denser medium, the reflection coefficient is high, and for rarer medium, the reflection coefficient is low.

$$Density \propto Reflection\ coefficient$$

When a medium is denser, the signal cannot penetrate through the medium. Hence, the signal gets reflected completely. If the medium is rarer, the signal penetrates completely through the medium.

Therefore,

$$and\ R = 0,\ for\ rarer\ medium$$
$$and\ R = 1,\ for\ denser\ medium$$

The above assumption is considered for mapping the image. The obtained reflection coefficient is related to the density to identify the sediment layer. The density values for different sediment layers are listed in Table 1.

Table 2 gives the typical values for different sediment textures and their density in **(g/cm^3)**. Marcelo Zeri et al. [16]. The reflection coefficient is mapped with density and is illustrated graphically in Fig 34. This implies the signal from the high-density material is reflected with a greater reflection coefficient.

TABLE 2. Sediment types and its Density

Sediment Type	Density
Clay	1.35
Clayey Sand	1.4
Sandy Clay	1.5
Coarse Sand	1.65
Exposed rock	2.65

Particle or Grain Size

The density of an object is related to the particle size of the object table 3. The denser objects are larger in size compared to the rarer medium. Hence, with the help of the density and particle size, the sediment layers are classified into sandy clay, clayey sand, coarse sand, exposed rock, etc.

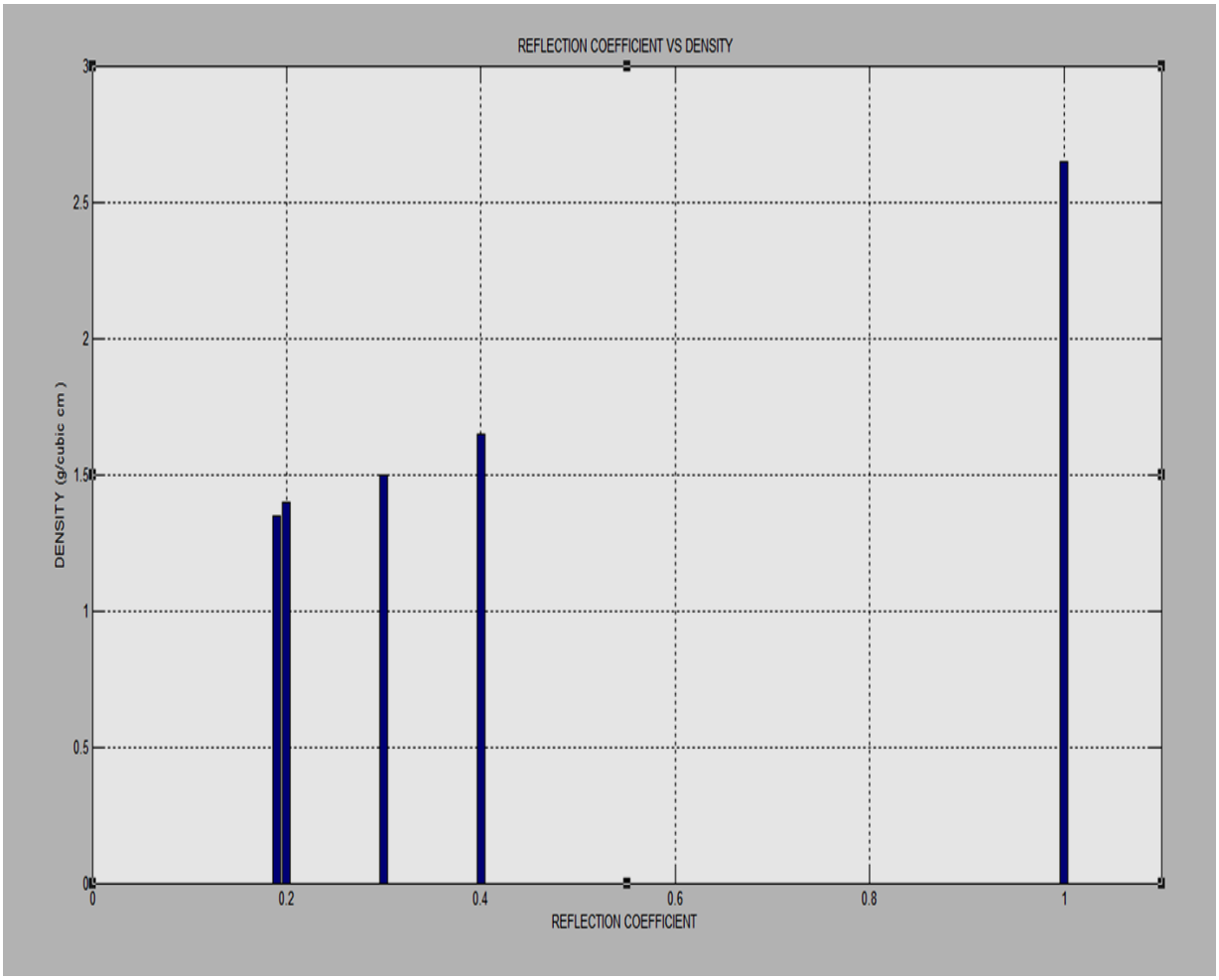

Fig 34. Reflection vs. Density

TABLE 3. Sediment types and their particle size

Sediment Type	Grain Size(mm)
Clay	Less than 0.002
Clayey sand	0.002-0.075
Sandy clay	0.002- 0.2
Coarse sand	2-4.75
Exposed rock	Greater than 300

According to the Indian Soil Classification System(ISSCS), sediments are classified with respect to grain size listed in Table 3 Sandy clay, clayey sand, coarse sand, exposed rock. (Ref http://www.soilmanagementindia.com/soil/soil-classification/basis-of-soil-classification/13460)[13].

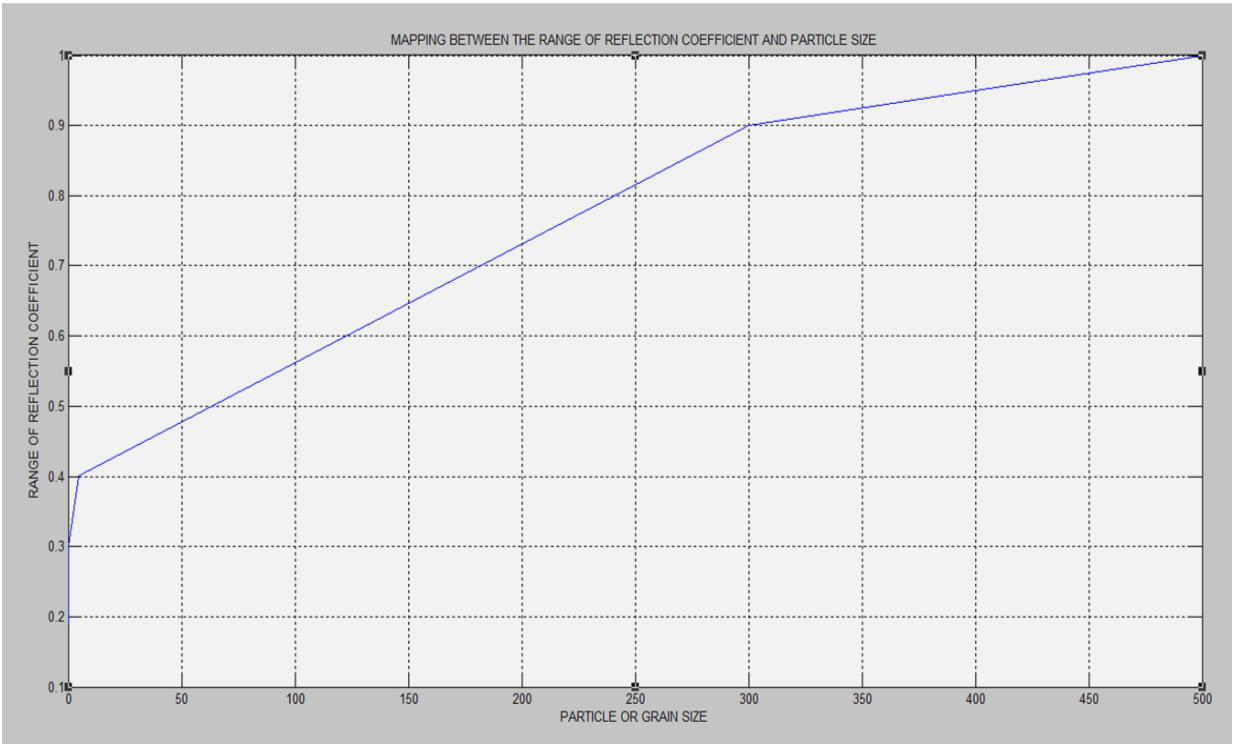

Fig 35 . Mapping between the range of Reflection Coefficient and Particle Size

Larger size particle has greater reflection. A linear graph is plotted, mapping particle size and reflection coefficient shown in Fig 35.

Table 4 gives the range of reflection coefficient values for the sediment layers obtained from the data. Based on the particle size, sediment layers are classified as sandy clay, clayey sand, coarse sand, exposed rock, illustrated in Fig 36.

Table 4. Reflection Coefficient VS Sediment Layers

Reflection Coefficient	Sediment Layers
0.9 – 1	Rock
0.3 to 0.4	Sandy Clay
0.2-0.3	Clayey Sand
0.19-0.2	Clay

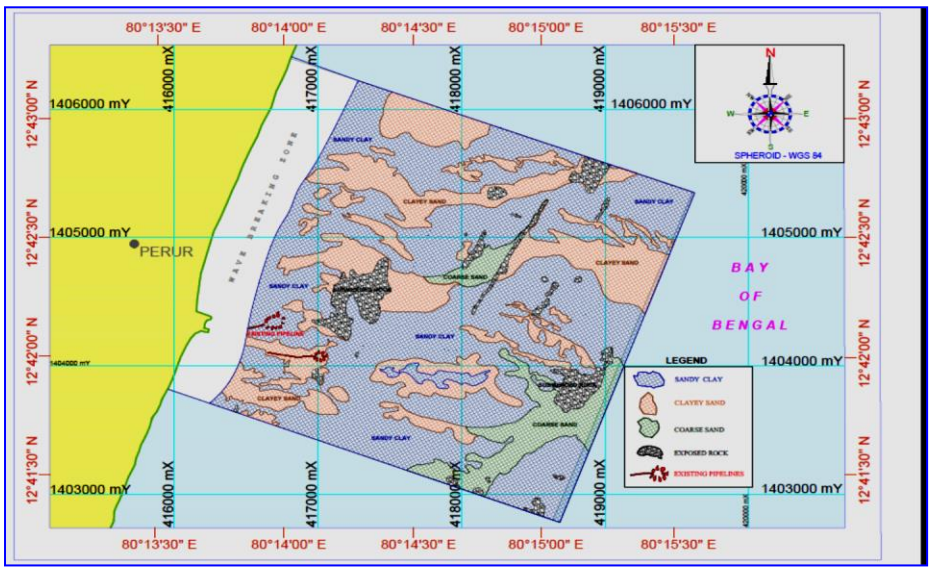

Fig 36. Classified map(Sediment Layers)

VI. CONCLUSION AND FUTURE WORK

In the geological survey, detection of rock category from overall sub-aquatic sediments as well as classification of sediments plays a significant component for lithologists. This research work is aimed at knowing the texture of soil from the image captured by the sub-bottom profiler before laying the pipelines. Thus the sediment layers are classified using CNN with Adam optimizer and analyzed based on reflectance properties assuming small reflection from smooth particles such as clay and high reflection from large particles of Rock. The deep learning-based 'SediDeep' model was developed for categorizing sediment particles such as coarse gravels, sands, clay, and other sediments in sea acoustics using side-scan sonar images. Moreover, the model was evaluated using CNN with Adam optimizer in the variation of learning rate as 0.01, 0.02, 0.03 to classify the sediments as rocks or sands. The metrics such as accuracy and loss were estimated during training as well as the testing phase to predict the overall model performance. Analysis of Pixel distribution in the classified sediment layers is implemented using the Reflection Coefficient parameter. The classified layers are mapped to their corresponding density values and to the particle size. Hence, we may conclude that Convnet with Adam optimizer is suitable for classifying sediment particles existing in the underwater sea; however, the experimental outcomes attains the classification accuracy as 90.27% using Adam optimizer with batch size 0.03 in grading sediments.

ACKNOWLEDGEMENT

The author would like to thank **INDOMER COASTAL HYDRAULICS PVT LTD** for providing the Sonar Image Data to carry out the research work. The authors also like to thank Dr. Chandra Mohan. P, INDOMER COASTAL HYDRAULICS PVT LTD, Mr.Baskaran, INDOMER COASTAL HYDRAULICS PVT LTD for their help in sonar image data acquisition

REFERENCES

[1] Caufield, D.d., Yim, Yung-Chang, Prediction of shallow sub-bottom sediment acoustic impedance while estimating absorption and other losses J.Canad. Soc. Explor. Geophys (1983).

[2] Hamilton, E.L. Bachman, R.T, Berger, W.H.Johnson, T.C.Mayer, Acoustic and related properties of calcareous deep-sea sediments, LA: Petrol 52, 733, 753(1982).

[3] Chivers R.C, Emerson N, Burns D, New acoustic processing for underway surveying Hydrogen. J., 42 (1990).

[4] Eleftherakis Dimitrios, AliReza, Amiri-Simkooei, Mirjam Snellen, Simons, Dick G., Improving riverbed sediment classification using backscatter and depth residual features of multi-beam echo-sounder systems, Acoust. Soc. Am., (2012).

[5] Amiri-Simkooei, Mirjam Snellen, Riverbed sediment classification using multi-beam echo-sounder backscatter data, J. Acoust. Soc. Am., 126(4) (2009) 1724–1738.

[6] Guillon Laurent, Lurton Xavier, Backscattering from buried sediment layers: The equivalent input backscattering strength mode, J. Acoust. Soc. Am., 109 (1) (2001).

[7] Hughes Clarke, J.E., Danforth, B.W., Valentine, P., Areal seabed classification using backscatter angular response at 95 kHz. Lerici, Italy: High-Frequency Acoustics in Shallow Water, NATO SACLANT Undersea Research Centre, (1997).

[8] A. Orłowski, Application of multiple echoes energy measurement for evaluation of bottom type, Oceanologia(1984).

[9] Preston, J.M., Christney, A.C., Beran, L.S., Collins, W.T., Statistical seabed segmentation e from images and echoes to objective clustering(2004).

[10] Sternlicht Daniel. D., De Moustier Christian. P, Time-dependent seafloor acoustic backscatter (10–100 kHz), Acoust. Soc. Am. (2003).

[11] D. R. Jackson, D. P. Winebrenner, and A. Ishimaru, Application of the composite roughness model to high-frequency bottom backscattering, J. Acoust. Soc. Am. 79(5) (1986) 1410–1422.

[12] Theuillon. G, Stéphan. Y., Pacault. A High-resolution geoacoustic characterization of the seafloor using a subbottom profiler, IEEE J. Ocean (2008).

[13] http://www.soilmanagementindia.com/soil/soil-classification/basis-of-soil-classification/13460

[14] Kumudham, R., Rajendran, V., Side Scan Sonar Image Data Mapping with Geographic Reference System, , Special Issue-21, Special Issue on Advance Engineering and Science 7(2.21) (2018) 410-413.

[15] Kumudham, R., Rajendran, V., Side-scan sonar image denoising and classification. Journal of Advanced Research in Dynamical & Control Systems, JARDCS, 13 (2017) 55-65.

[16] Marcelo Zeri , Regina Célia dos Santos Alvalá, Rogério Carneiro, Jose A Marengo, Tools for Communicating Agricultural Drought over the Brazilian Semiarid Using the Soil Moisture Index, (2018), Water 10(10):1421, DOI: 10.3390/w10101421.

[17] Berthold, T., Leichter, A., Rosenhahn, B., Berkhahn, V., & Valerius, J., Seabed sediment classification of side-scan sonar data using convolutional neural networks. (2017) IEEE Symposium Series on Computational Intelligence (SSCI). doi:10.1109/ssci.2017.8285220.

[18] Xiangjin Ran, Linfu Xue, Yanyan Zhang, Zeyu Liu, Xuejia Sang and Jinxin He, Rock Classification from Field Image Patches Analyzed Using a Deep Convolutional Neural Network, Mathematics, 7 (2019) 755. doi:10.3390/math7080755.

[19] Pierre Guy Atangana Njock, Qian Zheng, Ning Zang, Y-Shuang Xu, Perspective review in subsea jet trenching technology and modeling, Journal of marine science and engineering, J. Mar. Sci. Eng. 8 (2020) 460; doi:10.3390/jmse8060460.

[20] Daniel Ierodiaconou, Alexandre C. G. Schimel, David Kennedy, Jacquomo Monk, Grace Gaylard, Mary Young, Markus Diesing, Alex Rattray, Combining pixel and object-based image analysis of ultra-high resolution multibeam bathymetry and backscatter for habitat mapping in shallow marine waters Marine Geophysical Research, (2018), https://doi.org/10.1007/s11001-017-9338-z.

[21] Berthold, T., Leichter, A., Rosenhahn, B., Berkhahn, V., & Valerius, J., Seabed sediment classification of side-scan sonar data using convolutional neural networks. (2017) IEEE Symposium Series on Computational Intelligence (SSCI). doi:10.1109/ssci.2017.8285220

[22] Chen, J., & Zhang, S., Segmentation of Sonar Image on Seafloor Sediments Based on Multiclass SVM. Journal of Coastal Research, (2018) 597-602. Retrieved February 27, 2021, from https://www.jstor.org/stable/26543022

[23] Dell'Aversana, Paolo., Machine Learning for rock classification based on mineralogical and chemical composition. A tutorial (2018).

[24] E.E. Baraboshkin, L.S. Ismailova, D.M. Orlov, E.A. Zhukovskaya, G.A. Kalmykov, O.V. Khotylev, E.Yu. Baraboshkin, D.A. Koroteev Deep Convolutions for In-Depth Automated Rock Typing, arXiv:1909.10227 v 3 [cs.CV] 2 7 (2019).

[25] Frederick, C., Villar, S., & Michalopoulou, Z.-H., Seabed classification using physics-based modeling and machine learning, The Journal of the Acoustical Society of America, 148(2) (2020) 859–872. doi:10.1121/10.0001728.

Conflict of Interest: The authors declare that they have no conflict of interest.
This research did not receive any specific grant from funding agencies in the public, commercial, or not-for-profit sectors.

Ms.Radhika Surampudi is working as an Assistant professor in the Department of ECE at AMC Engineering College, Bengaluru. She did her B.Tech in Electronics and Communication Engineering in the year 2010 at Shri Vishnu Engineering College for women affiliated to JNTU Kakinada and M.Tech in VLSI Design in the year 2013 at Shri Vishnu Engineering College for women affiliated to JNTU Kakinada, and she is pursuing a Ph.D. in Vels Institute of Science Technology and Advanced Studies(VISTAS). Her Area of Interest is Image Processing, VLSI design, Internet of Things, Machine Learning. Email: radhika.surampudi@gmail.com.

Dr.R.Kumudham is working as an Assistant professor in the Department of Electronics and Communication Engineering at Vels Institute of Science Technology and Advanced Studies (VISTAS), Chennai. She completed her B.E. in Electronics and Communication Engineering in the year 2002 under Periyar University and M.E. (Communication Systems) in the year 2013 at Anna university. She completed her Ph.D. in VISTAS in the year 2020. Her area of interest is Image processing, Machine learning. She has published papers in IEEE Explore Digital Library, Web of Science, and Scopus indexed journals. **Corresponding Author: Email:** kumudham.se@velsuniv.ac.in/kumudham.rajamohan@gmail.com.

Dr.Ebenezer Abishek.B received his B.E in Electronics and Communication Engineering from Anna University, M.E in VLSI Design from Anna University, Chennai, and PhD in Electronics and Communication Engineering from Vels Institute of Science, Technology & Advanced Studies in 2010, 2012 and 2019 respectively. He is currently, working as an Associate Professor in the department of Electronics and Communication Engineering, Vels Institute of Science, Technology & Advanced Studies, Chennai with experience of 8 years and 8 months. He authored papers in reputed journals and international/national conferences. His area of interest includes Antennas & Propagation, Data Science, VLSI design and Wireless Communications. He has filed two national and one international patent. His ORCiD is 0000-0003-2908-7069.

Dr. V. Rajendran received his MTech in Physical Engineering from Indian Institute of Science, Bangalore, India and received hid PhD degree on Electrical and Electronics Engineering from Chiba University, Japan in 1981 and 1993, respectively. He is currently, a professor and the head of the department of Electronics and Communication Engineering in Vels Institute of Science and Technology, Pallavaram, Chennai, India. He was awarded MONBUSHO Fellowship, Japanese Govt. Fellowship (1988–1989) through the Ministry of Human Resource and Development, Govt. of India. He was elected twice as Vice Chairman – Asia of Execution Board of Data Buoy Co-operation Panel (DBCP) of Inter-Governmental Oceanographic Commission (IOC)/World Meteorological Organization (WMO) of UNSCO, in October 2008 and September 2009, respectively. He was a Life fellow of Ultrasonic Society of India, India (USI)in January 2001. He was a Life fellow of Institution of Electronics and Telecommunication Engineering (IETE), India, in January 2012. His area of interest includes cognitive radio and software-defined radio communication, antennas and propagation and wireless communication, under water acoustic signal processing and under water wireless networks. He has published 52 papers in web of science and Scopus-indexed journal. **Email:** director.ece@velsuniv.ac.in/drvrajen@gmail.com.